WORKSPACE ANALYSIS OF A NEW PARALLEL MANIPULATOR

M. Zaidie Abdul Majid, Zhen Huang, Y. Lawrence Yao
Department of Mechanical Engineering
Columbia University
New York, NY 10027

ABSTRACT

This paper studies the workspace of a six-DOF parallel manipulator of three-PPSR (prismatic-prismatic-spheric-revolute) type. It is well recognized that the most significant drawback of parallel manipulators is their limited workspace. To develop new parallel mechanisms with a larger workspace is of interest to additional applications. The mechanism of the three-PPSR manipulator and its variations are briefly analyzed first. The workspace is then determined and the effects of joint limit and limb interference constraints on the workspace shape and size are studied. The constituent regions of the workspace corresponding to different classes of manipulator poses are discussed. It is shown that the workspace of this parallel manipulator is larger than that of a comparable Stewart platform especially in the vertical direction.

INTRODUCTION

In the recent decade, many researchers have shown interest in parallel manipulators. Compared with the more commonly used serial manipulators, the parallel ones have attractive advantages in accuracy, rigidity, capacity and load-to-weight ratio. A parallel manipulator consists of a moving platform, a base platform and several branches connecting both platforms through appropriate kinematic joints with appropriate actuators. The most well-known parallel manipulator is the Stewart platform (Stewart, 1965), which has been widely studied. In a Stewart platform, six bars connecting moving and base platforms are extensible to control the position and orientation of the moving platform.

Many different six-DOF parallel manipulators have been proposed. More recently, a novel parallel manipulator is introduced and studied (Tsai and Tahmasebi, 1993; Tahmasebi and Tsai, 1994a, 1994b). This mechanism consists of an upper and a lower platforms and three inextensible limbs. The lower end of each limb connects through a ball-and-socket joint to an actuator. The actuator is of a linear stepper type but capable of moving in both x and y directions simultaneously on the base platform. The upper end of each limb is connected to the moving platform by a revolute joint. The manipulator is therefore a three-PPSR mechanism, where P denotes the prismatic pair, S the spherical pair, and R the revolute pair. The output motion of the planar linear stepping motors is similar to that of two cross prismatic pairs on the base platform. The desired motion of the upper platform is obtained by moving the actuators, to which the lower ends of the three limbs are attached, on the base platform. Besides the merits of the general parallel mechanisms over their serial counterparts mentioned before, this three-PPSR mechanism has added advantages, including simpler structure, and higher stiffness. It is also less likely for its limbs to interfere with each other, since it has only three inextensible instead of six extensible limbs as in a Stewart platform.

Tahmasebi and Tsai perceived this mechanism as being used as a minimanipulator, which can be mounted between the wrist and the end-effector of a serial manipulator for error compensation as well as delicate position and force control. Therefore, the required workspace is rather small such that the motion of each actuator is limited within a small circular area on the base platform when its workspace is considered (Tahmasebi and Tsai, 1994b). The actuators carrying the limbs, however, do not have to be so restricted, they can move over the entire base platform, resulting a much larger workspace. As a result, this three-PPSR mechanism can be used as a stand-alone manipulator. In addition, its special assembly of kinematic pairs makes it possible to have a much different and much larger workspace than that of a comparable Stewart platform. The study of workspace of a manipulator is one of the fundamental problems in the design of robot arms. As many researchers have pointed out, the major drawback of parallel mechanisms is their limited workspace. This three-PPSR parallel mechanism can help overcome the limitations of traditional parallel manipulators and extend the applications of parallel mechanisms. This paper analyzes the size, shape, composition, and constraints of the workspace of the three-PPSR parallel manipulator.

The workspace of parallel manipulators has attracted the attention of many researchers over the past decade. Much reported work on parallel mechanism workspace dealt with two-DOF or three-DOF planar and spherical manipulators. Asada and Ro (1985) analyzed the workspace of a closed-loop planar two-DOF five-bar parallel mechanism. Gosselin and Angeles (1989) studied the workspace of planar and spherical three-DOF mechanisms. Lee and Shah (1988) demonstrated the workspace of a spatial three-DOF in-parallel manipulator.

Much less work has been reported for the workspace of six-DOF parallel manipulators. Yang and Lee (1984), and Fichter (1986) described the workspace of the six-DOF parallel manipulators, through a method based on discretization of the Cartesian space. Gosselin (1990) used geometric properties to introduce an algorithm for determining the workspace of the six-DOF Stewart platform. His result showed that the workspace was the intersection of six annular regions. Masory and Wang (1992) more systematically studied the workspace of the six-DOF Stewart platform. Their report discussed several constraint conditions for calculating its workspace, including the region of rotational angle of kinematic pairs and the interference between any two limbs of the mechanism. In addition, they analyzed the shape of the workspace and the relationship between the workspace and the geometric parameters of the mechanism. Tahmasebi and Tsai (1994b) studied the workspace of this new three-PPSR parallel manipulator, where motion of each of the three actuators attached to the lower end of each limb is limited to a small circular area. This paper is focused on analyzing the workspace of the three-PPSR parallel manipulator. In the analysis, limb interference and joint limitations are considered, and the restrictions on the limb lower end movement is relaxed. Instead of allowing each actuator only to move within a small circle, all three actuators are allowed to move within a much large, common circle of diameter d (Fig. 1). The composition of the workspace is also studied by identifying constituent regions according to different classes of manipulator poses.

WORKSPACE ANALYSIS

A fixed reference frame $OXYZ$ is attached to the base platform as shown in Fig. 1. The origin O is located at the centroid of the large circle with diameter d. The X and Y axes lie on the same base platform and the Z axis is upward perpendicular to the base. The moving reference frame $Guvw$ is attached to the moving platform. The point G is located at the centroid of the equilateral triangle. The u axis is parallel with P_2P_3, and v axis passes through point P_1. The w axis is perpendicular to the moving plane.

To determine the workspace of a mechanism, its direct kinematics is normally needed. Inverse kinematics, however, has always been applied for this purpose when parallel mechanisms are concerned, although the inverse kinematics requires the use of a numerical solution. Given a pose (position and orientation) of the manipulator, the reference point of the upper platform determines an allowable point within the workspace, if the inverse kinematics of the given pose exists under all the kinematic constraints. By giving a series of poses and obtaining a series of allowable points of the upper platform, the workspace forms as the assembly of all the allowable points.

Inverse Kinematics

The coordinates of point P_i in the moving platform can be calculated via coordinate transformation when the pose of the upper platform is known. The orientation of the moving platform is given by Euler's angles yaw (θ_u), pitch (θ_v), and roll (θ_w). The coordinates of center point G

with respect to the fixed frame are X_g, Y_g and Z_g. The coordinate transformation matrix is $\mathrm{YPR}(\theta_u,\theta_v,\theta_w) =$

$$\begin{bmatrix} c\theta_v c\theta_w & s\theta_u s\theta_v c\theta_w - c\theta_u s\theta_w & c\theta_u s\theta_v c\theta_w + s\theta_u s\theta_w & x_g \\ c\theta_v s\theta_w & s\theta_u s\theta_v s\theta_w + c\theta_u c\theta_w & c\theta_u s\theta_v s\theta_w - s\theta_u c\theta_w & y_g \\ -s\theta_w & s\theta_v s\theta_w & c\theta_u c\theta_v & z_g \\ 0 & 0 & 0 & 1 \end{bmatrix} \quad (1)$$

where $s\theta = \sin\theta$ and $c\theta = \cos\theta$.

The coordinates of points P_1, P_2, and P_3 with respect to frame *Guvw* are

$$P'_1 = (0,\ m,\ 0)^T$$
$$P'_2 = (-1/2,\ -(1/2)\tan 30°,\ 0)^T \quad (2)$$
$$P'_3 = (1/2,\ -(1/2)\tan 30°,\ 0)^T$$

where $m = (1/2)\cos 30°$. The coordinates of point P_i with respect to the fixed frame are

$$P_i = \mathrm{YPR}(\theta_u,\ \theta_v,\ \theta_w)\begin{pmatrix} P'_i \\ 1 \end{pmatrix} \qquad i = 1, 2, 3 \quad (3)$$

From the geometry of the manipulator shown in Fig. 1, two simultaneous equations can be obtained. The first equation is

$$(x_{p,i} - x_{r,i})^2 + (y_{p,i} - y_{r,i})^2 + (z_{p,i} - k)^2 = r^2 \quad (4)$$

where constant k is the Z coordinate of point R_i. The subscripts p,i and r,i denote points P_i and R_i, respectively. This is the equation for a circle on the base. The second equation follows from the perpendicularity of vector $\mathbf{R}_i\mathbf{P}_i$ and vector $\mathbf{P}_{i+1}\mathbf{P}_{i+2}$. Since the joint at point P_i is revolute, point R_i is the intersection of the circle of Eq. (6) with the plane that contains vector $\mathbf{R}_i\mathbf{P}_i$ and is normal to vector $\mathbf{P}_{i+1}\mathbf{P}_{i+2}$. That is,

$$\begin{aligned} \mathbf{P}_{i+1}\mathbf{P}_{i+2} &= \langle n_x, n_y, n_z \rangle \\ &= \langle x_{p,i+2} - x_{p,i+1}, y_{p,i+2} - y_{p,i+1}, z_{p,i+2} - z_{p,i+1} \rangle \end{aligned} \quad (5)$$

The equation of the plane is given as

$$n_x(x_{p,i} - x_{r,i}) + n_y(y_{p,i} - y_{r,i}) + n_z(z_{p,i} - k) = 0 \quad (6)$$

Eqs. (4) and (6) are solved for $x_{r,i}$ and $y_{r,i}$,

$$\begin{aligned} x_{r,i} = [&-kn_x^2 n_z + n_x^3 x_{p,i} + n_x n_y^2 x_{p,i} + n_x^2 n_z z_{p,i} \\ &\mp n_x n_y (-k^2 n_x^2 - k^2 n_y^2 - k^2 n_z^2 + n_x^2 r^2 + \\ &n_y^2 r^2 + 2kn_x^2 z_{p,i} + 2kn_y^2 z_{p,i} + 2kn_z^2 z_{p,i} - \\ &n_x^2 z_{p,i}^2 - n_y^2 z_{p,i}^2 - n_z^2 z_{p,i}^2)^{0.5}] / [n_x^3 + n_x n_y^2] \\ y_{r,i} = [&-kn_y^2 n_z + n_x^2 y_{p,i} + n_y^2 y_{p,i} + n_y n_z z_{p,i} \\ &\pm n_x (-k^2 n_x^2 - k^2 n_y^2 - k^2 n_z^2 + n_x^2 r^2 + \\ &n_y^2 r^2 + 2kn_x^2 z_{p,i} + 2kn_y^2 z_{p,i} + 2kn_z^2 z_{p,i} - \\ &n_x^2 z_{p,i}^2 - n_y^2 z_{p,i}^2 - n_z^2 z_{p,i}^2)^{0.5}] / [n_x^2 + n_x n_y^2] \end{aligned} \quad (7)$$

Because Eq. (4) is a second-order polynomial, the $x_{r,i}$ and $y_{r,i}$ could have two values. These two values are valid as long as they satisfy the joint limit and interference conditions, and are within the allowable footprint space.

Kinematic Constraints

In determining the workspace of a three-PPSR manipulator, three types of kinematic constraints are considered. They are the diameter of the footprint circle, joint angle limits, and link interference.

Footprint Circle. The positions of the lower ends of all three limbs need to be inside the footprint circle (Fig. 1), that is

$$|\mathbf{R}_i| \le d/2 \quad (8)$$

where d is the diameter of the footprint circle and $\mathbf{R}_i$ denotes the radius vector of point R_i with respect to the origin O.

Joint Angle Constraints. The links are attached to the upper and lower plates by kinematic pairs which have physical limits. For instance, a ball joint is theoretically free to rotate 360° about each of the three orthogonal axes. In practice, however, its motion is restricted by the joint physical construction within a relatively small range. Thus, there is a need to impose the maximum rotational angle θ_{max} for each joint. The rotational angle and its limitation can be expressed as

$$\theta_i = \cos^{-1}((\mathbf{v}_i \bullet \mathbf{u}_i) / |\mathbf{v}_i|) \le \theta_{i,max} \quad (9)$$

where $\mathbf{v}_i$ is the vector of link l_i, and $\mathbf{u}_i$ is a vector representing the line which bisects the rotational range of each kinematic pair with respect to the fixed frame.

Link Interference. Since links have physical dimensions, interference might occur. Assume that each link is cylindrical with a diameter d_l, and D the shortest distance between two adjacent links l_i and l_{i+1}, the interference limitation can be expressed by

$$d_l \le D \quad (10)$$

The shortest distance between the center lines of two links is the length D_n of their common normal $\mathbf{n}_i$. That is

$$D_n = |\mathbf{n}_i \bullet \mathbf{P}_i\mathbf{P}_{i+1}| \quad (13)$$

where the unit vector $\mathbf{n}_i$ of the common normal direction between two adjacent links l_i and l_{i+1} can be obtained as

$$\mathbf{n}_i = (\mathbf{v}_i \times \mathbf{v}_{i+1}) / |\mathbf{v}_i \times \mathbf{v}_{i+1}| \quad (12)$$

Note that, the shortest distance between links is not always equal to the length D_n of the common normal. It could be larger than D_n. The shortest distance is the distance from point P_i to the link l_{i+1}, if the intersection point C_i of the link l_i and the common normal of the two links is situated beyond the link l_i itself, or the intersection point M_i of the link l_i and the perpendicular line from point P_{i+1} to link l_i is situated beyond link l_i itself. The shortest distance is directly the distance between the two end points P_i and P_{i+1}, if the two intersection points, M_i and M_{i+1}, are both beyond links l_i and l_{i+1}.

Three lines, including two adjacent links and their common normal, define two planes. The normals of these two planes are

$$\frac{\mathbf{n}_i \times \mathbf{v}_i}{|\mathbf{n}_i \times \mathbf{v}_i|} = \langle a_i, b_i, c_i \rangle$$
$$\frac{\mathbf{n}_i \times \mathbf{v}_{i+1}}{|\mathbf{n}_i \times \mathbf{v}_{i+1}|} = \langle a_{i+1}, b_{i+1}, c_{i+1} \rangle \tag{13}$$

The equations of the two planes are

$$a_i(x - x_{p,i}) + b_i(y - y_{p,i}) + c_i(z - z_{p,i}) = 0 \tag{14}$$
$$a_{i+1}(x - x_{p,i+1}) + b_{i+1}(y - y_{p,i+1}) + c_{i+1}(z - z_{p,i+1}) = 0 \tag{15}$$

A line in 3D space can be represented as

$$\frac{x - x_{p,i}}{v_{x,i}} = \frac{y - y_{p,i}}{v_{y,i}} = \frac{z - z_{p,i}}{v_{z,i}} \tag{16}$$

The equations of two center lines of two adjacent legs can be resolved from

$$v_{y,i}(x - x_{p,i}) - v_{x,i}(y - y_{p,i}) = 0 \tag{17}$$
$$v_{z,i}(y - y_{p,i}) - v_{y,i}(z - z_{p,i}) = 0 \tag{18}$$
$$v_{y,i+1}(x - x_{p,i+1}) - v_{x,i+1}(y - y_{p,i+1}) = 0 \tag{19}$$
$$v_{z,i+1}(y - y_{p,i+1}) - v_{y,i+1}(z - z_{p,i+1}) = 0 \tag{20}$$

where Eqs. 17 and 18 represent the center line of link l_i, and Eqs. 19 and 21 the center line of link l_{i+1}.

The intersection point C_i between line l_i and the common normal is obtained by solving Eqs. 15, 17 and 18 simultaneously,

$$\begin{aligned}
x_{intercept,i} = {} & [a_i v_{x,i+1} x_{p,i} + b_i(v_{y,i+1} x_{p,i+1} + v_{x,i+1} y_{p,i} \\
& - v_{x,i+1} y_{p,i+1}) + c_i(v_{z,i} x_{p,i+1} + v_{x,i+1} z_{p,i} - \\
& v_{x,i+1} z_{p,i+1})] / [a_i v_{x,i+1} + b_i v_{y,i+1} + c_i v_{z,i}] \\
y_{intercept,i} = {} & [a_i(v_{y,i+1} x_{p,i} - v_{y,i+1} x_{p,i+1} + v_{x,i+1} y_{p,i+1}) \\
& + b_i v_{y,i+1} y_{p,i} + c_i(v_{z,i} y_{p,i+1} + v_{y,i+1} z_{p,i} - \\
& v_{y,i+1} z_{p,i})] / [a_i v_{x,i+1} + b_i v_{y,i+1} + c_i v_{z,i}] \\
z_{intercept,i} = {} & [a_i(v_{z,i} x_{p,i} - v_{z,i} x_{p,i+1} + v_{x,i+1} z_{p,i+1}) \\
& + b_i(v_{z,i} y_{p,i} - v_{z,i} y_{p,i+1} + v_{y,i+1} z_{p,i+1}) + \\
& c_i v_{z,i} z_{p,i}] / [a_i v_{x,i+1} + b_i v_{y,i+1} + c_i v_{z,i}]
\end{aligned} \tag{21}$$

Eqs. 14, 19 and 20 are solved simultaneously to obtain the intersection point C_{i+1} on line $i+1$.

$$\begin{aligned}
x_{intercept,i+1} = {} & [a_{i+1} v_{x,i} x_{p,i+1} + b_{i+1}(v_{y,i} x_{p,i} + v_{x,i} y_{p,i+1} \\
& - v_{x,i} y_{p,i}) + c_{i+1}(v_{z,i+1} x_{p,i} + v_{x,i} z_{p,i+1} - \\
& v_{x,i} z_{p,i})] / [a_{i+1} v_{x,i} + b_{i+1} v_{y,i} + c_{i+1} v_{z,i+1}] \\
y_{intercept,i+1} = {} & [a_{i+1}(v_{y,i} x_{p,i+1} - v_{y,i} x_{p,i} + v_{x,i} y_{p,i}) \\
& + b_{i+1} v_{y,i} y_{p,i+1} + c_{i+1}(v_{z,i+1} y_{p,i} + v_{y,i} z_{p,i+1} - \\
& v_{y,i} z_{p,i+1})] / [a_{i+1} v_{x,i} + b_{i+1} v_{y,i} + c_{i+1} v_{z,i+1}] \\
z_{intercept,i+1} = {} & [a_{i+1}(v_{z,i+1} x_{p,i+1} - v_{z,i+1} x_{p,i} + v_{x,i} z_{p,i}) \\
& + b_{i+1}(v_{z,i+1} y_{p,i+1} - v_{z,i+1} y_{p,i} + v_{y,i} z_{p,i}) + \\
& c_{i+1} v_{z,i+1} z_{p,i+1}] / [a_{i+1} v_{x,i} + b_{i+1} v_{y,i} + c_{i+1} v_{z,i+1}]
\end{aligned} \tag{22}$$

For the three-PPSR mechanism considered in this paper, all six links are located between two plates. Interference is therefore impossible if $Z_{C_i} \geq Z_{P_i}$ and $Z_{C_{i+1}} \geq Z_{P_{i+1}}$.

NUMERICAL CASES & DISCUSSION

The workspace subject to the above-mentioned constraints is numerically studied. Each link is assumed to be cylindrical, and the geometric parameters are given as $r = 2.5$ units, $l = 1.0$ units, $d = 6$ units, $d_l = 0.15$ units, $\theta_{r,max} = 75°$, $\theta_{s,max} = 60°$, and $k = 0$, where r denotes the leg length of P_iR_i, l the length of each side of the moving triangle, d the diameter of the footprint circle on the base platform, d_l the diameter of the links. $\theta_{r,max}$ and $\theta_{s,max}$ are the allowable maximum angles of rotation for the revolute joint and the spherical joint, respectively, and constant k denotes the Z coordinate of point R_i.

The three-dimensional workspace is presented in two graphical forms, i.e., a two-dimensional topview, and a three-dimensional isometric view of the workspace boundary without showing the upper and lower portions of the boundary for viewing convenience. Since the workspace involves both position and orientation, it has six dimensions in nature and therefore three invariable Euler's angles are specified for each case below. In order to demonstrate different situations and the effects of constraints on workspace size and shape, five typical cases are studied,

Case 1 : $\{\theta_u, \theta_v, \theta_w\} = \{0, 0, 0\}$

Case 2 : $\{\theta_u, \theta_v, \theta_w\} = \{20, 0, 0\}$

Case 3 : $\{\theta_u, \theta_v, \theta_w\} = \{-20, 0, 0\}$

Case 4 : $\{\theta_u, \theta_v, \theta_w\} = \{0, 20, 0\}$

Case 5 : $\{\theta_u, \theta_v, \theta_w\} = \{20, 20, 0\}$

Please note that, since the platform is symmetric about the v-axis of the moving platform, the case of $\{\theta_u, \theta_v, \theta_w\} = \{0°, -20°, 0°\}$ will be the same as $\{\theta_u, \theta_v, \theta_w\} = \{0°, 20°, 0°\}$. In addition, θ_w remains zero in all five cases because the shape of the workspace will remain the same for any θ_w value. This is in turn because the workspace will simply rotate by θ_w for any non-zero θ_w value without shape change.

Fig. 2 shows the topview of the workspace for case 1 where $\{\theta_u, \theta_v, \theta_w\} = \{0°, 0°, 0°\}$. Fig. 3 includes isometric views of the practical workspace for cases 1 and 5 where all the kinematic constraints are considered. It is seen that the shapes and the structures of the workspaces of this three-PPSR parallel mechanism are completely different from that of traditional parallel mechanisms. It especially allows a larger range of motion in the Z direction.

It should be pointed out that the actual shape of the reachable workspace of this parallel manipulator is not these shown in Fig. 3, where θ_w has been kept zero. Since θ_w can rotate by 360°, the actual shape of the workspace is resulted by rotating the shape shown in Fig. 3 about the Z axis for 360° (Fig. 4). Comparing with a comparable Stewart platform, which usually has a workspace in the shape of a mushroom cap, this workspace has a cylindrical shape and therefore a larger Z range as well. This will have significance in some applications.

The workspace is further examined to understand its composition. The examination is achieved through decomposing the workspace into its constituent regions according to different classes of manipulator poses. The workspace shown in Fig. 2 (case 1) is used as an example. Let $Z = 1.0$ for the system, four types of regions which constitute the workspace can be identified: 1) region that corresponds to the pose in which one leg points toward the platform and the other two legs point outward from the platform; 2) region that corresponds to the pose in which two legs point toward the platform while the third points outward from the platform; 3) region that corresponds to the pose in which all three legs point toward the platform; and 4) region that corresponds to the pose in which all three legs point outward from the platform. The fourth type of region has no practical effect on workspace determination since it is always a subset of the type-3 region. All these regions are plotted in Fig. 5, where a footprint circle of diameter of 6 units is also plotted. It is clear that the intersection of these regions forms an area which is identical to that shown in Fig. 2. It is, therefore, clear that they are the constituent regions of the workspace.

CONCLUSION

In this paper, the workspace of the three-PPSR manipulator is analyzed. It is shown that the workspace consists of three types of regions, each corresponding to a class of manipulator poses. The effects of various kinematic constraints, including revolute and spherical joint limitations and limb interference on workspace structure are numerically explored. In terms of size, the three-PPSR manipulator has a larger workspace than that of a comparable Stewart platform. Its actual workspace assumes a cylindrical shape while a Stewart platform usually has a mushroom-cap type of workspace which only allows limited motion in the Z direction.

REFERENCES

Asada, H., Ro, I. H., "A linkage design for direct drive robot arms," *J. of Mech. Trans. Aut. in Design*, Vol. 107, 536-540, 1985.

Fichter, E. F., "A Steward platform-based manipulator: general theory and practical construction," *The Int. J. of Rob. Res*, 5(2). 157-182, 1986.

Gosselin, C., "Determination of the workspace of six-DOF parallel manipulator," *J. of Mechanical Design* , Vol. 112, 331-336, 1990.

Gosselin, C., Angeles, J., "The optimum kinematic design of a spherical three-DOF parallel manipulator." *J. of Mech. Trans. Aut. in Des*, Vol. 111, 202-207, 1989.

Lee, K. M., Shah, D. K., "Kinematic analysis of a three-DOF in-parallel actuated manipulator," *IEEE J. of Rob. and Aut.* 4(3), 354-360, 1988.

Masory, O., Wang, J., "Workspace evaluation of Stewart platform," *Proc. ASME WAM*, DE-Vol. 45, 337-352, 1992.

Stewart, D., "A platform with six degrees of freedom," Proc. Institute of Mechanical Engr., London, England, Vol. 180, 25-28, 1965.

Tahmasebi, F., Tsai, L. -W., "Closed-form direct kinematics solution of a new parallel manipulator," *J. of Mechanical Design*, Vol. 116, 1141-1147, 1994a.

Tahmasebi, F., Tsai, L. -W., "Workspace and singularity analysis of a novel six-DOF parallel manipulator," *J. of Applied Mechanisms & Robotics*, Vol. 1 No. 2, 31-40, 1994b.

Tsai, L. -W., Tahmasebi, F., "Synthesis and analysis of a new class of six- DOF parallel manipulators," *J. of Robotic Systems*, Vol. 10, 561-580, 1993.

Yang, D. C. H., Lee, T. W., "Feasibility study of a platform type of robotic manipulators from a kinematic viewpoint," *J. of Mech. Trans. Aut. in Des.*, Vol. 106, 191-198, 1984.

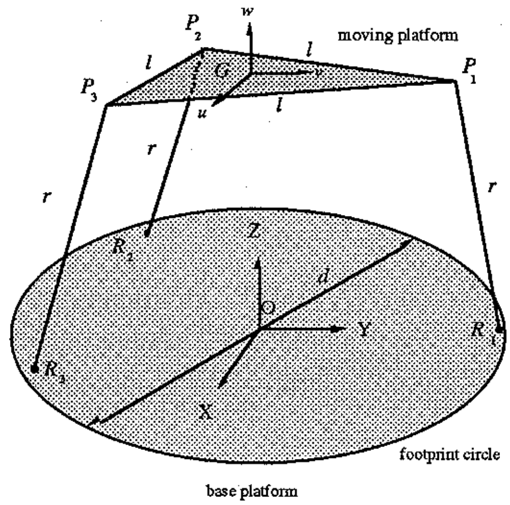

FIG. 1 THREE-PPSR PARALLEL MANIPULATOR.

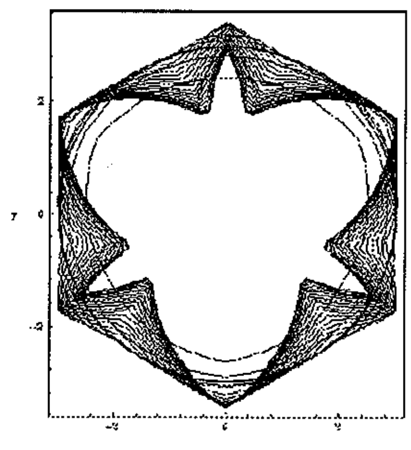

FIG. 2 TOPVIEW OF WORKSPACE (CASE 1: $\{\theta_U, \theta_V, \theta_W\} = \{0°, 0°, 0°\}$)

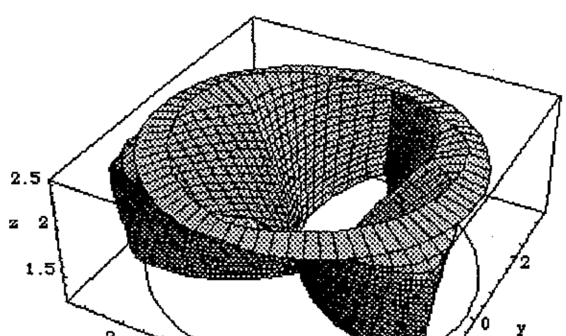

(A) CASE 1: $\{\theta_U, \theta_V, \theta_W\} = \{0°, 0°, 0°\}$

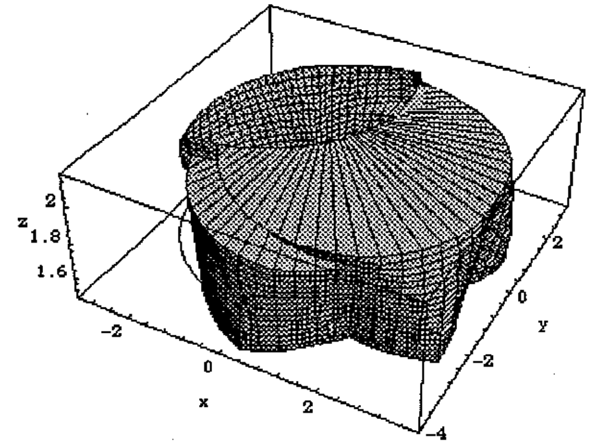

(B) CASE 5: $\{\theta_U, \theta_V, \theta_W\} = \{20°, 20°, 0°\}$

FIG. 3 WORKSPACE BOUNDARY WITH JOINT LIMIT AND INTERFERENCE CONSTRAINTS (THE TOP AND BOTTOM PLATES OF THE BOUNDARY NOT SHOWN FOR VIEWING CONVENIENCE)

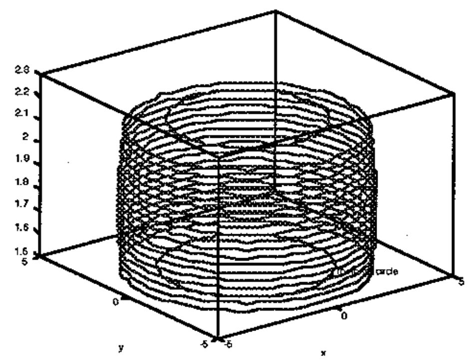

FIG. 4 ACTUAL WORKSPACE BY REVOLVING THE BOUNDARY SHOWN IN FIG. 3B ABOUT THE Z AXIS FOR 360° (CASE 5)

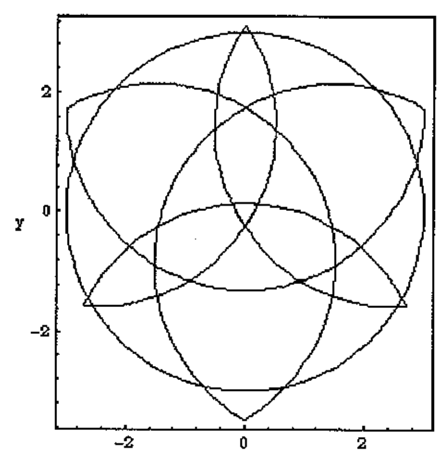

FIG. 5 INTERSECTION OF THE CONSTITUENT REGIONS FORMS THE WORKSPACE (CASE 1) WITH FOOTPRINT CIRCLE SHOWN

WORKSPACE ANALYSIS OF A NEW PARALLEL MANIPULATOR

M. Zaidie Abdul Majid, Zhen Huang, Y. Lawrence Yao
Department of Mechanical Engineering
Columbia University
New York, NY 10027

ABSTRACT

This paper studies the workspace of a six-DOF parallel manipulator of three-PPSR (prismatic-prismatic-spheric-revolute) type. It is well recognized that the most significant drawback of parallel manipulators is their limited workspace. To develop new parallel mechanisms with a larger workspace is of interest to additional applications. The mechanism of the three-PPSR manipulator and its variations are briefly analyzed first. The workspace is then determined and the effects of joint limit and limb interference constraints on the workspace shape and size are studied. The constituent regions of the workspace corresponding to different classes of manipulator poses are discussed. It is shown that the workspace of this parallel manipulator is larger than that of a comparable Stewart platform especially in the vertical direction.

INTRODUCTION

In the recent decade, many researchers have shown interest in parallel manipulators. Compared with the more commonly used serial manipulators, the parallel ones have attractive advantages in accuracy, rigidity, capacity and load-to-weight ratio. A parallel manipulator consists of a moving platform, a base platform and several branches connecting both platforms through appropriate kinematic joints with appropriate actuators. The most well-known parallel manipulator is the Stewart platform (Stewart, 1965), which has been widely studied. In a Stewart platform, six bars connecting moving and base platforms are extensible to control the position and orientation of the moving platform.

Many different six-DOF parallel manipulators have been proposed. More recently, a novel parallel manipulator is introduced and studied (Tsai and Tahmasebi, 1993; Tahmasebi and Tsai, 1994a, 1994b). This mechanism consists of an upper and a lower platforms and three inextensible limbs. The lower end of each limb connects through a ball-and-socket joint to an actuator. The actuator is of a linear stepper type but capable of moving in both x and y directions simultaneously on the base platform. The upper end of each limb is connected to the moving platform by a revolute joint. The manipulator is therefore a three-PPSR mechanism, where P denotes the prismatic pair, S the spherical pair, and R the revolute pair. The output motion of the planar linear stepping motors is similar to that of two cross prismatic pairs on the base platform. The desired motion of the upper platform is obtained by moving the actuators, to which the lower ends of the three limbs are attached, on the base platform. Besides the merits of the general parallel mechanisms over their serial counterparts mentioned before, this three-PPSR mechanism has added advantages, including simpler structure, and higher stiffness. It is also less likely for its limbs to interfere with each other, since it has only three inextensible instead of six extensible limbs as in a Stewart platform.

Tahmasebi and Tsai perceived this mechanism as being used as a minimanipulator, which can be mounted between the wrist and the end-effector of a serial manipulator for error compensation as well as delicate position and force control. Therefore, the required workspace is rather small such that the motion of each actuator is limited within a small circular area on the base platform when its workspace is considered (Tahmasebi and Tsai, 1994b). The actuators carrying the limbs, however, do not have to be so restricted, they can move over the entire base platform, resulting a much larger workspace. As a result, this three-PPSR mechanism can be used as a stand-alone manipulator. In addition, its special assembly of kinematic pairs makes it possible to have a much different and much larger workspace than that of a comparable Stewart platform. The study of workspace of a manipulator is one of the fundamental problems in the design of robot arms. As many researchers have pointed out , the major drawback of parallel mechanisms is their limited workspace. This three-PPSR parallel mechanism can help overcome the limitations of traditional parallel manipulators and extend the applications of parallel mechanisms. This paper analyzes the size, shape, composition, and constraints of the workspace of the three-PPSR parallel manipulator.

The workspace of parallel manipulators has attracted the attention of many researchers over the past decade. Much reported work on parallel mechanism workspace dealt with two-DOF or three-DOF planar and spherical manipulators. Asada and Ro (1985) analyzed the workspace of a closed-loop planar two-DOF five-bar parallel mechanism. Gosselin and Angeles (1989) studied the workspace of planar and spherical three-DOF mechanisms. Lee and Shah (1988) demonstrated the workspace of a spatial three-DOF in-parallel manipulator.

Much less work has been reported for the workspace of six-DOF parallel manipulators. Yang and Lee (1984) , and Fichter (1986) described the workspace of the six-DOF parallel manipulators, through a method based on discretization of the Cartesian space. Gosselin (1990) used geometric properties to introduce an algorithm for determining the workspace of the six-DOF Stewart platform. His result showed that the workspace was the intersection of six annular regions. Masory and Wang (1992) more systematically studied the workspace of the six-DOF Stewart platform. Their report discussed several constraint conditions for calculating its workspace, including the region of rotational angle of kinematic pairs and the interference between any two limbs of the mechanism. In addition, they analyzed the shape of the workspace and the relationship between the workspace and the geometric parameters of the mechanism. Tahmasebi and Tsai (1994b) studied the workspace of this new three-PPSR parallel manipulator, where motion of each of the three actuators attached to the lower end of each limb is limited to a small circular area. This paper is focused on analyzing the workspace of the three-PPSR parallel manipulator. In the analysis, limb interference and joint limitations are considered, and the restrictions on the limb lower end movement is relaxed. Instead of allowing each actuator only to move within a small circle, all three actuators are allowed to move within a much large, common circle of diameter d (Fig. 1). The composition of the workspace is also studied by identifying constituent regions according to different classes of manipulator poses.

WORKSPACE ANALYSIS

A fixed reference frame $OXYZ$ is attached to the base platform as shown in Fig. 1. The origin O is located at the centroid of the large circle with diameter d. The X and Y axes lie on the same base platform and the Z axis is upward perpendicular to the base. The moving reference frame $Guvw$ is attached to the moving platform. The point G is located at the centroid of the equilateral triangle. The u axis is parallel with P_2P_3, and v axis passes through point P_1. The w axis is perpendicular to the moving plane.

To determine the workspace of a mechanism, its direct kinematics is normally needed. Inverse kinematics, however, has always been applied for this purpose when parallel mechanisms are concerned, although the inverse kinematics requires the use of a numerical solution. Given a pose (position and orientation) of the manipulator, the reference point of the upper platform determines an allowable point within the workspace, if the inverse kinematics of the given pose exists under all the kinematic constraints. By giving a series of poses and obtaining a series of allowable points of the upper platform, the workspace forms as the assembly of all the allowable points.

Inverse Kinematics

The coordinates of point P_i in the moving platform can be calculated via coordinate transformation when the pose of the upper platform is known. The orientation of the moving platform is given by Euler's angles yaw (θ_u), pitch (θ_v), and roll (θ_w). The coordinates of center point G

with respect to the fixed frame are X_g, Y_g and Z_g. The coordinate transformation matrix is $\mathrm{YPR}(\theta_u, \theta_v, \theta_w) =$

$$\begin{bmatrix} c\theta_v c\theta_w & s\theta_u s\theta_v c\theta_w - c\theta_u s\theta_w & c\theta_u s\theta_v c\theta_w + s\theta_u s\theta_w & x_g \\ c\theta_v s\theta_w & s\theta_u s\theta_v s\theta_w + c\theta_u c\theta_w & c\theta_u s\theta_v s\theta_w - s\theta_u c\theta_w & y_g \\ -s\theta_w & s\theta_v s\theta_w & c\theta_u c\theta_v & z_g \\ 0 & 0 & 0 & 1 \end{bmatrix} \quad (1)$$

where $s\theta = \sin\theta$ and $c\theta = \cos\theta$.

The coordinates of points P_1, P_2, and P_3 with respect to frame *Guvw* are

$$P'_1 = (0, m, 0)^T$$
$$P'_2 = (-l/2,\ -(l/2)\tan 30°,\ 0)^T \quad (2)$$
$$P'_3 = (l/2,\ -(l/2)\tan 30°,\ 0)^T$$

where $m = (l/2)\cos 30°$. The coordinates of point P_i with respect to the fixed frame are

$$P_i = \mathrm{YPR}(\theta_u, \theta_v, \theta_w)\begin{pmatrix} P_i' \\ 1 \end{pmatrix} \qquad i = 1, 2, 3 \quad (3)$$

From the geometry of the manipulator shown in Fig. 1, two simultaneous equations can be obtained. The first equation is

$$(x_{p,i} - x_{r,i})^2 + (y_{p,i} - y_{r,i})^2 + (z_{p,i} - k)^2 = r^2 \quad (4)$$

where constant k is the Z coordinate of point R_i. The subscripts p,i and r,i denote points P_i and R_i, respectively. This is the equation for a circle on the base. The second equation follows from the perpendicularity of vector $\mathbf{R}_i\mathbf{P}_i$ and vector $\mathbf{P}_{i+1}\mathbf{P}_{i+2}$. Since the joint at point P_i is revolute, point R_i is the intersection of the circle of Eq. (6) with the plane that contains vector $\mathbf{R}_i\mathbf{P}_i$ and is normal to vector $\mathbf{P}_{i+1}\mathbf{P}_{i+2}$. That is,

$$\mathbf{P}_{i+1}\mathbf{P}_{i+2} = \langle n_x, n_y, n_z \rangle$$
$$= \langle x_{p,i+2} - x_{p,i+1}, y_{p,i+2} - y_{p,i+1}, z_{p,i+2} - z_{p,i+1} \rangle \quad (5)$$

The equation of the plane is given as

$$n_x(x_{p,i} - x_{r,i}) + n_y(y_{p,i} - y_{r,i}) + n_z(z_{p,i} - k) = 0 \quad (6)$$

Eqs. (4) and (6) are solved for $x_{r,i}$ and $y_{r,i}$,

$$\begin{aligned} x_{r,i} = [&-kn_x^2 n_z + n_x^3 x_{p,i} + n_x n_y^2 x_{p,i} + n_x^2 n_z z_{p,i} \\ &\mp n_x n_y(-k^2 n_x^2 - k^2 n_y^2 - k^2 n_z^2 + n_x^2 r^2 + \\ &n_y^2 r^2 + 2kn_x^2 z_{p,i} + 2kn_y^2 z_{p,i} + 2kn_z^2 z_{p,i} - \\ &n_x^2 z_{p,i}^2 - n_y^2 z_{p,i}^2 - n_z^2 z_{p,i}^2)^{0.5}] / [n_x^3 + n_x n_y^2] \\ y_{r,i} = [&-kn_y^2 n_z + n_x^2 y_{p,i} + n_y^2 y_{p,i} + n_y n_z z_{p,i} \\ &\pm n_x(-k^2 n_x^2 - k^2 n_y^2 - k^2 n_z^2 + n_x^2 r^2 + \\ &n_y^2 r^2 + 2kn_x^2 z_{p,i} + 2kn_y^2 z_{p,i} + 2kn_z^2 z_{p,i} - \\ &n_x^2 z_{p,i}^2 - n_y^2 z_{p,i}^2 - n_z^2 z_{p,i}^2)^{0.5}] / [n_x^2 + n_x n_y^2] \end{aligned} \quad (7)$$

Because Eq. (4) is a second-order polynomial, the $x_{r,i}$ and $y_{r,i}$ could have two values. These two values are valid as long as they satisfy the joint limit and interference conditions, and are within the allowable footprint space.

Kinematic Constraints

In determining the workspace of a three-PPSR manipulator, three types of kinematic constraints are considered. They are the diameter of the footprint circle, joint angle limits, and link interference.

Footprint Circle. The positions of the lower ends of all three limbs need to be inside the footprint circle (Fig. 1), that is

$$|\mathbf{R}_i| \le d/2 \quad (8)$$

where d is the diameter of the footprint circle and $\mathbf{R}_i$ denotes the radius vector of point R_i with respect to the origin O.

Joint Angle Constraints. The links are attached to the upper and lower plates by kinematic pairs which have physical limits. For instance, a ball joint is theoretically free to rotate 360° about each of the three orthogonal axes. In practice, however, its motion is restricted by the joint physical construction within a relatively small range. Thus, there is a need to impose the maximum rotational angle θ_{max} for each joint. The rotational angle and its limitation can be expressed as

$$\theta_i = \cos^{-1}((\mathbf{v}_i \bullet \mathbf{u}_i) / |\mathbf{v}_i|) \le \theta_{i,max} \quad (9)$$

where $\mathbf{v}_i$ is the vector of link l_i, and $\mathbf{u}_i$ is a vector representing the line which bisects the rotational range of each kinematic pair with respect to the fixed frame.

Link Interference. Since links have physical dimensions, interference might occur. Assume that each link is cylindrical with a diameter d_l, and D the shortest distance between two adjacent links l_i and l_{i+1}, the interference limitation can be expressed by

$$d_l \le D \quad (10)$$

The shortest distance between the center lines of two links is the length D_n of their common normal $\mathbf{n}_i$. That is

$$D_n = |\mathbf{n}_i \bullet \mathbf{P}_i\mathbf{P}_{i+1}| \quad (13)$$

where the unit vector $\mathbf{n}_i$ of the common normal direction between two adjacent links l_i and l_{i+1} can be obtained as

$$\mathbf{n}_i = (\mathbf{v}_i \times \mathbf{v}_{i+1}) / |\mathbf{v}_i \times \mathbf{v}_{i+1}| \quad (12)$$

Note that, the shortest distance between links is not always equal to the length D_n of the common normal. It could be larger than D_n. The shortest distance is the distance from point P_i to the link l_{i+1}, if the intersection point C_i of the link l_i and the common normal of the two links is situated beyond the link l_i itself, or the intersection point M_i of the link l_i and the perpendicular line from point P_{i+1} to link l_i is situated beyond link l_i itself. The shortest distance is directly the distance between the two end points P_i and P_{i+1}, if the two intersection points, M_i and M_{i+1}, are both beyond links l_i and l_{i+1}.

Three lines, including two adjacent links and their common normal, define two planes. The normals of these two planes are

$$\frac{\mathbf{n}_i \times \mathbf{v}_i}{|\mathbf{n}_i \times \mathbf{v}_i|} = \langle a_i, b_i, c_i \rangle$$
$$\frac{\mathbf{n}_i \times \mathbf{v}_{i+1}}{|\mathbf{n}_i \times \mathbf{v}_{i+1}|} = \langle a_{i+1}, b_{i+1}, c_{i+1} \rangle \qquad (13)$$

The equations of the two planes are

$$a_i(x - x_{p,i}) + b_i(y - y_{p,i}) + c_i(z - z_{p,i}) = 0 \qquad (14)$$
$$a_{i+1}(x - x_{p,i+1}) + b_{i+1}(y - y_{p,i+1}) + c_{i+1}(z - z_{p,i+1}) = 0 \qquad (15)$$

A line in 3D space can be represented as

$$\frac{x - x_{p,i}}{v_{x,i}} = \frac{y - y_{p,i}}{v_{y,i}} = \frac{z - z_{p,i}}{v_{z,i}} \qquad (16)$$

The equations of two center lines of two adjacent legs can be resolved from

$$v_{y,i}(x - x_{p,i}) - v_{x,i}(y - y_{p,i}) = 0 \qquad (17)$$
$$v_{z,i}(y - y_{p,i}) - v_{y,i}(z - z_{p,i}) = 0 \qquad (18)$$
$$v_{y,i+1}(x - x_{p,i+1}) - v_{x,i+1}(y - y_{p,i+1}) = 0 \qquad (19)$$
$$v_{z,i+1}(y - y_{p,i+1}) - v_{y,i+1}(z - z_{p,i+1}) = 0 \qquad (20)$$

where Eqs. 17 and 18 represent the center line of link l_i, and Eqs. 19 and 21 the center line of link l_{i+1}.

The intersection point C_i between line l_i and the common normal is obtained by solving Eqs. 15, 17 and 18 simultaneously,

$$\begin{aligned}
x_{intercept,i} &= [a_i v_{x,i+1} x_{p,i} + b_i(v_{y,i+1} x_{p,i+1} + v_{x,i+1} y_{p,i} \\
&\quad - v_{x,i+1} y_{p,i+1}) + c_i(v_{z,i} x_{p,i+1} + v_{x,i+1} z_{p,i} - \\
&\quad v_{x,i+1} z_{p,i+1})] / [a_i v_{x,i+1} + b_i v_{y,i+1} + c_i v_{z,i}] \\
y_{intercept,i} &= [a_i(v_{y,i+1} x_{p,i} - v_{y,i+1} x_{p,i+1} + v_{x,i+1} y_{p,i+1}) \\
&\quad + b_i v_{y,i+1} y_{p,i} + c_i(v_{z,i} y_{p,i+1} + v_{y,i+1} z_{p,i} - \\
&\quad v_{y,i+1} z_{p,i})] / [a_i v_{x,i+1} + b_i v_{y,i+1} + c_i v_{z,i}] \\
z_{intercept,i} &= [a_i(v_{z,i} x_{p,i} - v_{z,i} x_{p,i+1} + v_{x,i+1} z_{p,i+1}) \\
&\quad + b_i(v_{z,i} y_{p,i} - v_{z,i} y_{p,i+1} + v_{y,i+1} z_{p,i+1}) + \\
&\quad c_i v_{z,i} z_{p,i}] / [a_i v_{x,i+1} + b_i v_{y,i+1} + c_i v_{z,i}]
\end{aligned} \qquad (21)$$

Eqs. 14, 19 and 20 are solved simultaneously to obtain the intersection point C_{i+1} on line $i+1$.

$$\begin{aligned}
x_{intercept,i+1} &= [a_{i+1} v_{x,i} x_{p,i+1} + b_{i+1}(v_{y,i} x_{p,i} + v_{x,i} y_{p,i+1} \\
&\quad - v_{x,i} y_{p,i}) + c_{i+1}(v_{z,i+1} x_{p,i} + v_{x,i} z_{p,i+1} - \\
&\quad v_{x,i} z_{p,i})] / [a_{i+1} v_{x,i} + b_{i+1} v_{y,i} + c_{i+1} v_{z,i+1}] \\
y_{intercept,i+1} &= [a_{i+1}(v_{y,i} x_{p,i+1} - v_{y,i} x_{p,i} + v_{x,i} y_{p,i}) \\
&\quad + b_{i+1} v_{y,i} y_{p,i+1} + c_{i+1}(v_{z,i+1} y_{p,i} + v_{y,i} z_{p,i+1} - \\
&\quad v_{y,i} z_{p,i+1})] / [a_{i+1} v_{x,i} + b_{i+1} v_{y,i} + c_{i+1} v_{z,i+1}] \\
z_{intercept,i+1} &= [a_{i+1}(v_{z,i+1} x_{p,i+1} - v_{z,i+1} x_{p,i} + v_{x,i} z_{p,i}) \\
&\quad + b_{i+1}(v_{z,i+1} y_{p,i+1} - v_{z,i+1} y_{p,i} + v_{y,i} z_{p,i}) + \\
&\quad c_{i+1} v_{z,i+1} z_{p,i+1}] / [a_{i+1} v_{x,i} + b_{i+1} v_{y,i} + c_{i+1} v_{z,i+1}]
\end{aligned} \qquad (22)$$

For the three-PPSR mechanism considered in this paper, all six links are located between two plates. Interference is therefore impossible if $Z_{C_i} \geq Z_{P_i}$ and $Z_{C_{i+1}} \geq Z_{P_{i+1}}$.

NUMERICAL CASES & DISCUSSION

The workspace subject to the above-mentioned constraints is numerically studied. Each link is assumed to be cylindrical, and the geometric parameters are given as $r = 2.5$ units, $l = 1.0$ units, $d = 6$ units, $d_l = 0.15$ units, $\theta_{r,max} = 75°$, $\theta_{s,max} = 60°$, and $k = 0$, where r denotes the leg length of P_iR_i, l the length of each side of the moving triangle, d the diameter of the footprint circle on the base platform, d_l the diameter of the links. $\theta_{r,max}$ and $\theta_{s,max}$ are the allowable maximum angles of rotation for the revolute joint and the spherical joint, respectively, and constant k denotes the Z coordinate of point R_i.

The three-dimensional workspace is presented in two graphical forms, i.e., a two-dimensional topview, and a three-dimensional isometric view of the workspace boundary without showing the upper and lower portions of the boundary for viewing convenience. Since the workspace involves both position and orientation, it has six dimensions in nature and therefore three invariable Euler's angles are specified for each case below. In order to demonstrate different situations and the effects of constraints on workspace size and shape, five typical cases are studied,

Case 1 : $\{\theta_u, \theta_v, \theta_w\} = \{0, 0, 0\}$

Case 2 : $\{\theta_u, \theta_v, \theta_w\} = \{20, 0, 0\}$

Case 3 : $\{\theta_u, \theta_v, \theta_w\} = \{-20, 0, 0\}$

Case 4 : $\{\theta_u, \theta_v, \theta_w\} = \{0, 20, 0\}$

Case 5 : $\{\theta_u, \theta_v, \theta_w\} = \{20, 20, 0\}$

Please note that, since the platform is symmetric about the v-axis of the moving platform, the case of $\{\theta_u, \theta_v, \theta_w\} = \{0°, -20°, 0°\}$ will be the same as $\{\theta_u, \theta_v, \theta_w\} = \{0°, 20°, 0°\}$. In addition, θ_w remains zero in all five cases because the shape of the workspace will remain the same for any θ_w value. This is in turn because the workspace will simply rotate by θ_w for any non-zero θ_w value without shape change.

Fig. 2 shows the topview of the workspace for case 1 where $\{\theta_u, \theta_v, \theta_w\} = \{0°, 0°, 0°\}$. Fig. 3 includes isometric views of the practical workspace for cases 1 and 5 where all the kinematic constraints are considered. It is seen that the shapes and the structures of the workspaces of this three-PPSR parallel mechanism are completely different from that of traditional parallel mechanisms. It especially allows a larger range of motion in the Z direction.

It should be pointed out that the actual shape of the reachable workspace of this parallel manipulator is not these shown in Fig. 3, where θ_w has been kept zero. Since θ_w can rotate by 360°, the actual shape of the workspace is resulted by rotating the shape shown in Fig. 3 about the Z axis for 360° (Fig. 4). Comparing with a comparable Stewart platform, which usually has a workspace in the shape of a mushroom cap, this workspace has a cylindrical shape and therefore a larger Z range as well. This will have significance in some applications.

The workspace is further examined to understand its composition. The examination is achieved through decomposing the workspace into its constituent regions according to different classes of manipulator poses. The workspace shown in Fig. 2 (case 1) is used as an example. Let Z = 1.0 for the system, four types of regions which constitute the workspace can be identified: 1) region that corresponds to the pose in which one leg points toward the platform and the other two legs point outward from the platform; 2) region that corresponds to the pose in which two legs point toward the platform while the third points outward from the platform; 3) region that corresponds to the pose in which all three legs point toward the platform; and 4) region that corresponds to the pose in which all three legs point outward from the platform. The fourth type of region has no practical effect on workspace determination since it is always a subset of the type-3 region. All these regions are plotted in Fig. 5, where a footprint circle of diameter of 6 units is also plotted. It is clear that the intersection of these regions forms an area which is identical to that shown in Fig. 2. It is, therefore, clear that they are the constituent regions of the workspace.

CONCLUSION

In this paper, the workspace of the three-PPSR manipulator is analyzed. It is shown that the workspace consists of three types of regions, each corresponding to a class of manipulator poses. The effects of various kinematic constraints, including revolute and spherical joint limitations and limb interference on workspace structure are numerically explored. In terms of size, the three-PPSR manipulator has a larger workspace than that of a comparable Stewart platform. Its actual workspace assumes a cylindrical shape while a Stewart platform usually has a mushroom-cap type of workspace which only allows limited motion in the Z direction.

REFERENCES

Asada, H., Ro, I. H., "A linkage design for direct drive robot arms," *J. of Mech. Trans. Aut. in Design*, Vol. 107, 536-540, 1985.

Fichter, E. F., "A Steward platform-based manipulator: general theory and practical construction," *The Int. J. of Rob. Res*, 5(2). 157-182, 1986.

Gosselin, C., "Determination of the workspace of six-DOF parallel manipulator," *J. of Mechanical Design*, Vol. 112, 331-336, 1990.

Gosselin, C., Angeles, J., "The optimum kinematic design of a spherical three-DOF parallel manipulator." *J. of Mech. Trans. Aut. in Des*, Vol. 111, 202-207, 1989.

Lee, K. M., Shah, D. K., "Kinematic analysis of a three-DOF in-parallel actuated manipulator," *IEEE J. of Rob. and Aut.* 4(3), 354-360, 1988.

Masory, O., Wang, J., "Workspace evaluation of Stewart platform," *Proc. ASME WAM*, DE-Vol. 45, 337-352, 1992.

Stewart, D., "A platform with six degrees of freedom," Proc. Institute of Mechanical Engr., London, England, Vol. 180, 25-28, 1965.

Tahmasebi, F., Tsai, L. -W., "Closed-form direct kinematics solution of a new parallel manipulator," *J. of Mechanical Design*, Vol. 116, 1141-1147, 1994a.

Tahmasebi, F., Tsai, L. -W., "Workspace and singularity analysis of a novel six-DOF parallel manipulator," *J. of Applied Mechanisms & Robotics*, Vol. 1 No. 2, 31-40, 1994b.

Tsai, L. -W., Tahmasebi, F., "Synthesis and analysis of a new class of six- DOF parallel manipulators," *J. of Robotic Systems*, Vol. 10, 561-580, 1993.

Yang, D. C. H., Lee, T. W., "Feasibility study of a platform type of robotic manipulators from a kinematic viewpoint," *J. of Mech. Trans. Aut. in Des.*, Vol. 106, 191-198, 1984.

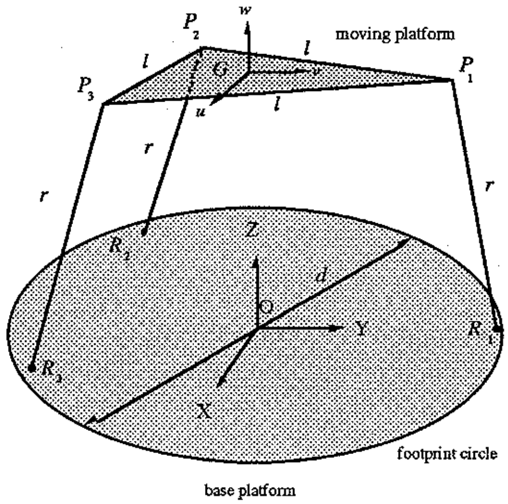

FIG. 1 THREE-PPSR PARALLEL MANIPULATOR.

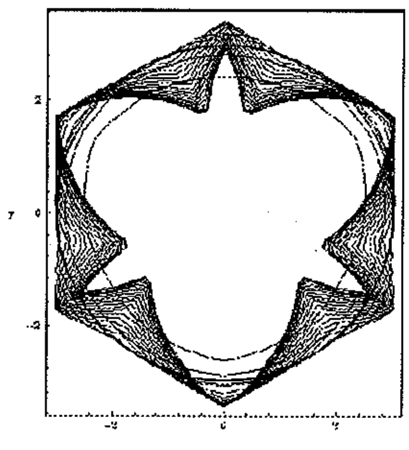

FIG. 2 TOPVIEW OF WORKSPACE (CASE 1: $\{\theta_U, \theta_V, \theta_W\} = \{0°, 0°, 0°\}$)

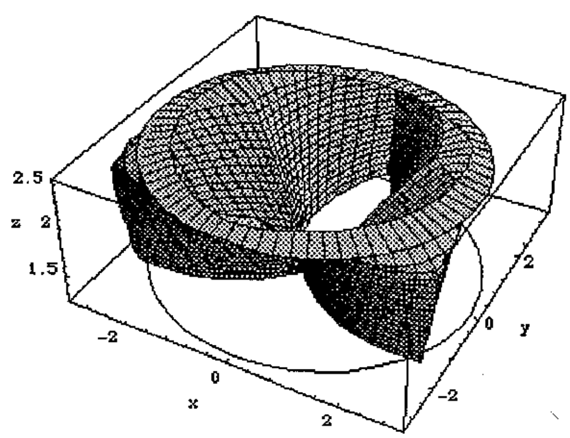

(A) CASE 1: $\{\theta_U, \theta_V, \theta_W\} = \{0°, 0°, 0°\}$

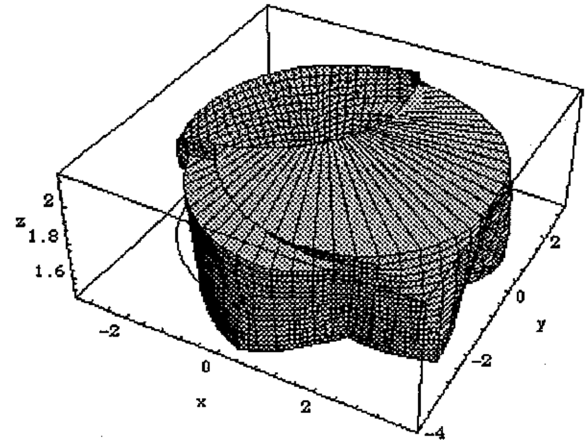

(B) CASE 5: $\{\theta_U, \theta_V, \theta_W\} = \{20°, 20°, 0°\}$

FIG. 3 WORKSPACE BOUNDARY WITH JOINT LIMIT AND INTERFERENCE CONSTRAINTS (THE TOP AND BOTTOM PLATES OF THE BOUNDARY NOT SHOWN FOR VIEWING CONVENIENCE)

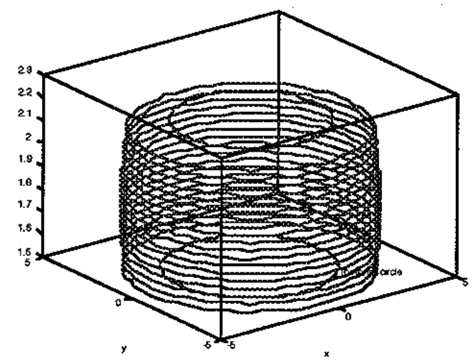

FIG. 4 ACTUAL WORKSPACE BY REVOLVING THE BOUNDARY SHOWN IN FIG. 3B ABOUT THE Z AXIS FOR 360° (CASE 5)

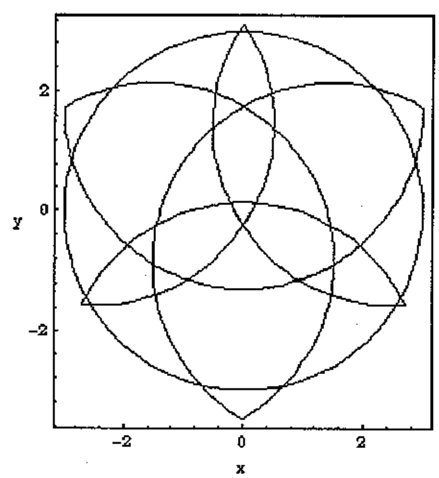

FIG. 5 INTERSECTION OF THE CONSTITUENT REGIONS FORMS THE WORKSPACE (CASE 1) WITH FOOTPRINT CIRCLE SHOWN